Structure and optical properties of semiconductor quantum nanostructures self-formed in inverted tetrahedral pyramids

1999 J. Phys.: Condens. Matter 11 5901

(http://iopscience.iop.org/0953-8984/11/31/302)

J. Phys.: Condens. Matter **11** (1999) 5901–5915. Printed in the UK PII: S0953-8984(99)02121-9

Structure and optical properties of semiconductor quantum nanostructures self-formed in inverted tetrahedral pyramids

A Hartmann, Y Ducommun, K Leifer and E Kapon

Physics Department, Swiss Federal Institute of Technology (EPFL), CH-1015 Lausanne, Switzerland

Received 24 February 1999

Abstract. We present a method for fabricating quantum dots using seeded self-organized growth of GaAs/AlGaAs heterostructures on substrates patterned with inverted pyramids. This method produces, at the tip of each inverted pyramid, highly uniform quantum dots whose size and position can be accurately controlled. In addition, a system of connected GaAs and AlGaAs two- and one-dimensional nanostructures is identified in the inverted pyramids using cross-sectional atomic force microscopy. A substrate removal technique is used to optimally prepare our samples for optical studies, allowing the increase of the luminescence efficiency of the quantum dots by up to three orders of magnitude. Micro-photoluminescence and cathodo-luminescence spectroscopy are used to study in detail the bandgap structure of the connected nanostructures identified in the pyramids, which constitute a complex, but controlled, barrier environment for the quantum dots.

1. Introduction

Semiconductor quantum dots (QDs) constitute an interesting low-dimensional system in which trapped charge carriers (electrons, holes, excitons and exciton complexes) are quantum confined in all three spatial directions [1]. Unlike 'natural' atoms and molecules, the characteristics of the confining potential of these 'artificial atoms and molecules' can be modified, allowing the investigation of structures beyond the conventional Coulomb potential case. Furthermore, the fact that these dots are incorporated in a solid state (semiconductor) matrix makes possible studies of the effect of the environment, e.g., interaction with lattice excitations such as phonons, excitons etc in the vicinity of the dot on the confined particles inside the dot. Such effects do not have a direct analogue in conventional atomic or molecular physics and are thus expected to yield new physics and further insight into the properties of low-dimensional systems.

In addition to the interesting physics involved, the realization and understanding of QD systems with controllable structural features will permit the assessment of their application in novel electronic and optical devices which utilize both their atomic-like properties and the fact that they are inserted in a solid state matrix. Among these applications one can mention QD lasers, which should show extremely low threshold and improved dynamic features [2, 3], and cellular automata dot array structures for advanced computer architectures [4–6].

The most widely used method to date for producing QD structures with good interface quality relies on strain-induced self-ordering of island-like structures using the Stranski–Krastanow growth mode [7–12]. This approach yields dots with very high density ($\sim 10^{10}$ cm^{-2}) exhibiting a broad size distribution and located at random sites. Vertical alignment of such dots using the residual strain fields above each dot has been demonstrated

0953-8984/99/315901+15$30.00

[13–15]. Several approaches for producing QD structures with more controlled potential wells and positioning have also been explored, most notably laser induced disordering of QW structures [16, 17] and cleaved edge overgrowth [18, 19]. The former approach, however, is limited to relatively large dots whereas the latter suffers from extremely small (a few meV) potential well depths.

Our approach is based on a different type of semiconductor QD heterostructure fabrication technique, namely seeded self-ordering on non-planar substrates [20, 21]. High-quality one-dimensional QWRs grown in V-grooved patterns have already been demonstrated with this approach [22–27]. This approach has been extended to realize QD heterostructures, e.g., using self-limited growth in inverted pyramids [28, 29]. The features of the self-ordering involved in the formation of such dots make possible the control of the potential well over a wide range of parameters. Moreover, the QD heterostructures exhibit a distinct set of low-dimensional barriers (bulk, quantum wells and quantum wires) which should permit the studies of the effect of barrier dimensionality on the electronic properties of the dots. This approach thus yields dots with highly controlled environments. The full control of the dot position makes possible its placement in such a way that local probing of the dot and its environment becomes relatively easy using rather conventional experimental techniques.

The aim of this paper is to give a detailed overview of the structural and optical properties of connected quantum nanostructures grown in inverted pyramids. Our results should serve as a basis for obtaining further insight into the physical properties of QDs in a complex yet controlled environment.

The paper is organized as follows. In section 2, we describe our sample preparation and growth methods, and discuss the resulting three-dimensional growth evolution inside the pyramids as observed by atomic force microscopy (AFM). A typical optical spectrum of a single pyramidal structure is presented in section 3. An advanced sample preparation technique, the so-called 'back-etching' method, is then described in section 3.1. This technique allows us to gain several orders of magnitude in the luminescence efficiency of the QD. Section 3.2 is devoted to a detailed study of the bandgap structure of the complex system of connected nanostructures present in the pyramids, using low-temperature micro-photoluminescence (μPL) and cathodoluminescence (CL) spectroscopy. All features in the optical spectra are identified in accordance with the structural study made earlier. In section 3.3, we focus on more specific experiments on single QDs, demonstrating, e.g., the uniformity of our dots across mm^2 areas and our ability to tailor the QD bandgap over more than 120 meV.

2. Structural characterization

The preparation of our samples relies on optical lithography. Pyramidal recess patterns are wet-etched on (111)B GaAs substrates using Br_2:methanol through an SiO_2 mask, resulting in sharp-tip, inverted pyramids delimited by three (111)A straight sidewalls (figure 1(a)). GaAs/AlGaAs heterostructures are then grown using low-pressure (20 mbar) organo-metallic chemical vapour deposition (LP-OMCVD), at a temperature of 650 °C [29]. The faceting of the grown layers inside the pyramids was studied by plan view scanning electron microscopy (SEM) (figure 1(b)). The (111)A sidewalls of the as-etched pyramids evolve during growth into a pair of vicinal (111)A planes, whose angles of misorientation were deduced to be $8.5 \pm 1^\circ$ and $5 \pm 2^\circ$ in the (111)B surface and the (110) plane, respectively [29].

The three-dimensional growth evolution in our pyramidal substrate patterns and the resulting complex system of nanostructures was studied by cross sectional AFM (x-AFM) [29, 30]. Figure 2 shows an example of x-AFM images of an AlGaAs/GaAs/AlGaAs multiple QW growth study, illustrating the very regular microstructure obtained under optimized growth

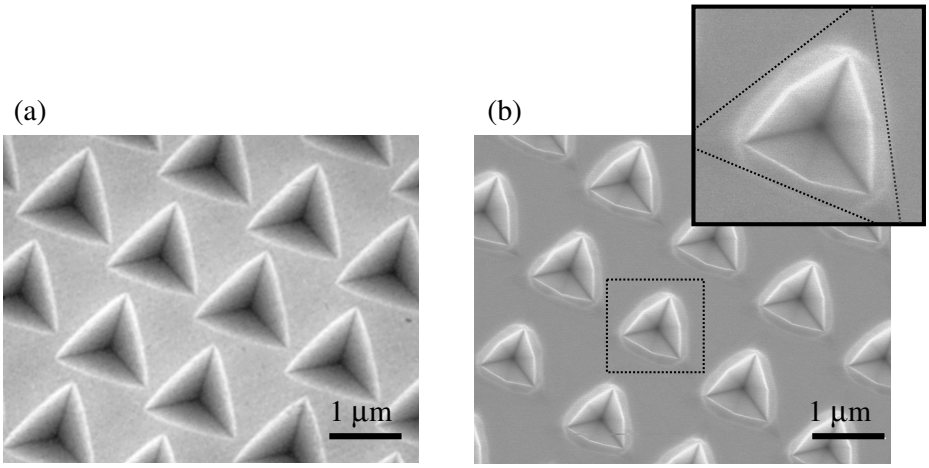

Figure 1. SEM top views of a 2 μm pitch pyramid array (a) before growth and (b) after growth of an AlGaAs/GaAs sequence. Inset: magnified view of an inverted pyramid after growth, showing the as-etched (111)A planes and the vicinal (111)A planes developing during growth.

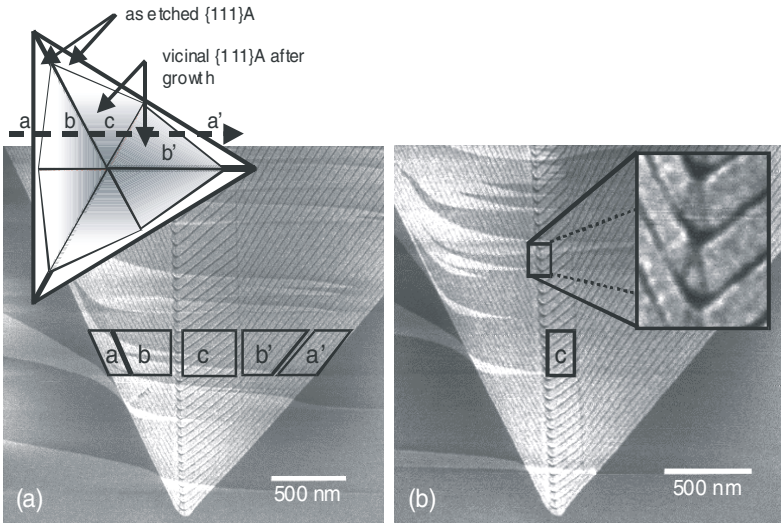

Figure 2. x-AFM images showing the regular growth evolution of AlGaAs (light grey) and GaAs (dark grey) in the pyramidal holes. The as-etched (111)A planes (marked 'a', see also top-view schematic illustration in the left inset) are replaced during growth by vicinal (111)A planes 'b', 'c' and 'b'. The magnified view of the principal corner between facets 'b' and 'c' in the right inset demonstrates how the self-limited growth evolution makes possible a vertical stacking of QWRs and QDs. Also the two branches of the vertical Ga-rich AlGaAs QW (VQW) are clearly observed.

conditions. Clearly visible is the self-ordered nature of the growth evolution at the pyramid corners. While deposition of GaAs leads to a thickening of the GaAs layer at this point, i.e. formation of a QWR, subsequent growth of AlGaAs reduces the radius of curvature at the corner back to its original, self-limiting value, and the vertical stacking of identical nanostructures becomes possible. The formation of a vertical Ga-rich AlGaAs QW (VQW) is clearly observed as well in such x-AFM images.

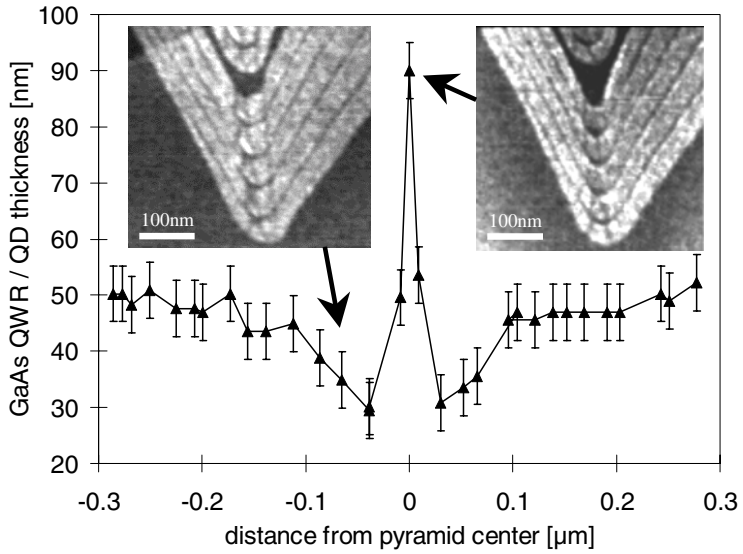

Figure 3. Thickness of the GaAs QWRs, measured along the pyramid corners, plotted as a function of the distance from the pyramid centre (tip of the pyramid) as obtained from subsequent x-AFM images taken along a cleaved edge. The QD at the pyramid centre (x-AFM image in right inset) is approximately a factor of two thicker than the QWR (left inset). The QWR thickness increases with the distance from the centre (tapering of QWR) [31].

Figure 3 summarizes an extensive x-AFM study of the thickness distribution of the GaAs QWR as a function of the distance from the pyramid centre [31]. As a main result, we found the thickness ratio between the GaAs QW on the pyramid sidewalls, the QWR along the pyramid corners and the QD at the pyramid tip to be approximately 1:3:6. In addition, we observe a characteristic tapering of the QWR. Its thickness increases with increasing distance from the pyramid centre. This QWR tapering has been observed also in photo- and cathodoluminescence studies, as further discussed below.

The structural results of our x-AFM studies are summarized in figure 4. Deposition of a GaAs QW layer results in 'lateral' QWs on the pyramid sidewalls, 'lateral' QWRs along the pyramid corners and the QD at the tip of the pyramid. In addition, the self-limited growth leads also to the formation of nanostructures during the deposition of the AlGaAs barrier layers. Here, vertical, Ga-rich AlGaAs QWs (VQWs) along the pyramid corners [32] and a vertical, Ga-rich AlGaAs QWR (VQWR) at the centre of the pyramid are formed.

3. Optical characterization

Figure 5(a) shows a typical low-temperature μPL spectrum of a single pyramid [31]. Here, we identified the different spectral contributions by their energy positions and the expected GaAs thicknesses, as determined using a simple square well model, neglecting lateral quantization. We obtained approximately 1, 3.5 and 6 nm for the high-, middle- and low-energy peaks, respectively. These thicknesses correspond rather well to the ratio of 1:3:6 for QW:QWR:QD expected from the x-AFM studies. Figure 5(b) shows a μPL image, in which the exciting laser light has been filtered out. The bright spot unambiguously indicates that the luminescence is indeed emitted by one single pyramid. Several other experiments, like excitation power dependent measurements, showing a strong saturation at high powers for the QD contribution,

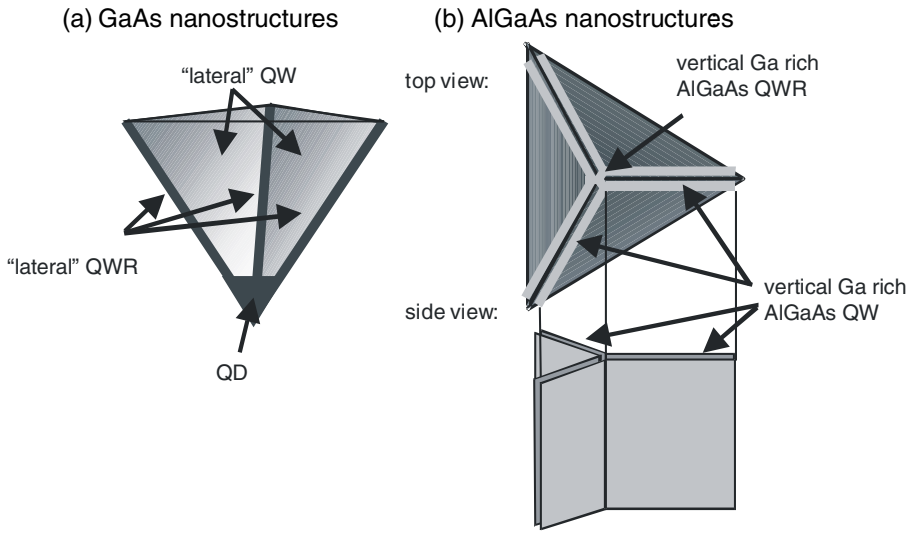

Figure 4. Schematic diagrams of the different GaAs (a) and AlGaAs (b) nanostructures formed by self-limited growth in the pyramidal recesses.

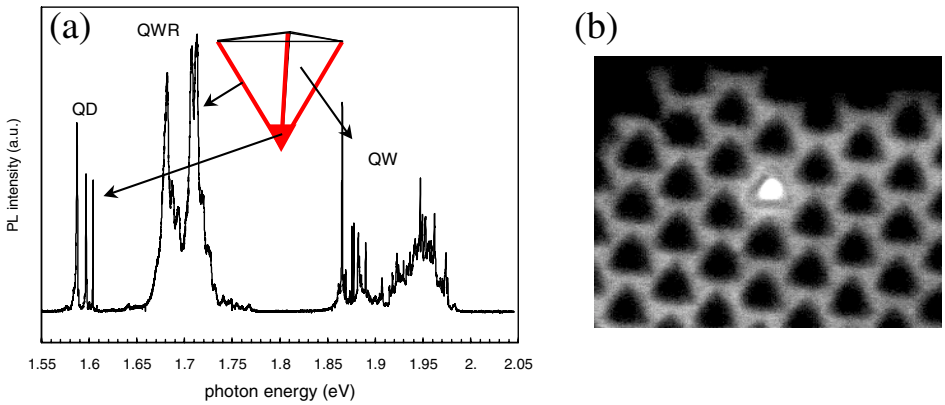

Figure 5. (a) μPL spectrum of a single pyramidal pattern containing a single GaAs QW layer (10 K, 10 μW excitation, laser spot 1 μm^2, pyramid array pitch: 1.4 μm). According to their energy positions and the corresponding GaAs thicknesses estimated using a simple square well model, we attribute the different peaks to the QD (low energy, ∼6 nm thickness), the GaAs QWR (medium energy, ∼3.5 nm) and a mixture of GaAs QW (∼1 nm) and AlGaAs VQW (high-energy) features, as indicated. (b) PL emission microscopic image of a 5.5 μm pitch array of pyramids, showing that the luminescence is emitted by one single pyramid.

cleaved edge measurements and μPL line-scans, were used to further substantiate these peak assignments (see below).

Direct evidence for the assignment of the QWR transition is given by the PL spectra and simultaneously recorded images, taken using a larger (∼15 μm) laser spot (figure 6). In the images, the luminescence is seen as a triplet of bright spots located at the corners of each pyramid. Since this is exactly the place where the QWR emission is expected, we assign the dominating peak in the spectra to the QWRs. The QWR emission is located at the upper parts

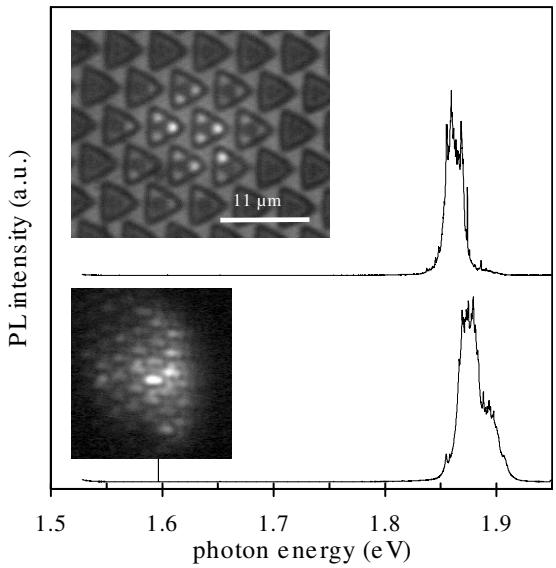

Figure 6. μPL of 5.5 μm (top) and 2.5 μm (bottom) pitch pyramids using a $\sim$15 μm laser spot and the corresponding PL images. The triplet of bright spots for each pyramid in the PL image can be attributed to the three QWRs along the pyramid corners. Therefore, the dominant peak in the PL spectra can be assigned to the QWRs.

of the pyramids due to the tapering of its thickness, as already observed in x-AFM images (see section 2). A detailed discussion of the tapering of the QWR, as studied by μPL and CL, will be the subject of section 3.2.2. In the sample of figure 6, the QW is extremely thin and its emission is therefore quite weak.

3.1. Advanced sample preparation: 'back-etching' process

Due to the inverted pyramid geometry, reflection and refraction processes may limit the QD PL efficiency. Indeed, most of the light emitted form the QD could be totally internally reflected by the steep pyramid sidewall surfaces and therefore could not escape from the structure. In a PL experiment, refraction at these steep pyramid sidewalls could also guide the incident light of the exciting laser away from the QD, leading to a lower concentration of excited carriers in the QD environment.

On the other hand, if the GaAs substrate is removed and the pyramid turned upside down, the sidewalls should act as a built-in lens, allowing more light to escape from the semiconductor QD (even as compared with a planar surface). Similarly, an incident exciting laser beam would be preferentially focused to the area around the QD (see schematics in figure 7(d)). This idea led us to develop the 'back-etching' technique: As a first step of the process, a gold layer is deposited on the sample surface. This layer supports and holds together the individual pyramids after the substrate removal, reflects light that would otherwise be lost to this side of the sample and is potentially usable as a contact layer. Next, the sample is glued upside down on a silicon support. After the back side of the GaAs substrate is mechanically polished down to 40–70 μm, the remaining GaAs substrate is etched away using an NH_4OH:H_2O_2 solution in a home-built jet-etching setup. We found that an NH_4OH:H_2O_2 mixing ratio of 1:30 is sufficiently selective to stop at a 100 nm thick etch stop layer of $Al_{0.55}Ga_{0.45}As$.

3.2. Optical properties of back-etched pyramids

3.2.1. Strong enhancement of QD luminescence efficiency. A typical 'back-etched' pyramid sample is shown in the SEM image of figure 7(a). The hollow AlGaAs pyramid is resting on a gold support and the pyramid tip, containing the QD, is facing upward. The uniformity of the 'back-etching' process is demonstrated by the large-area SEM image of figure 7(b).

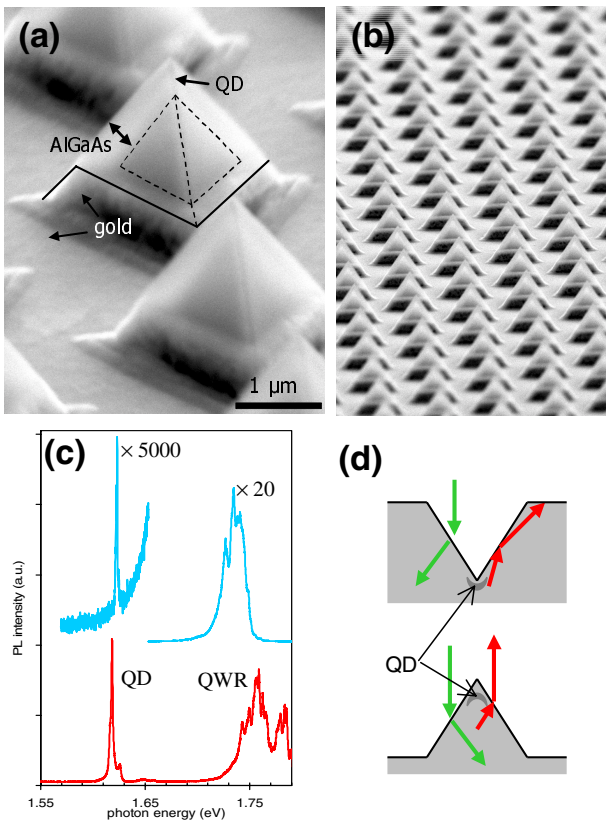

Figure 7. (a), (b) SEM images of 'back-etched' pyramids. (c) Comparison of μPL spectra of single pyramids of the same sample before (top) and after (bottom) the 'back-etching' process. (d) Schematics of the propagation of light rays in the pyramids; top—inverted pyramid structure, bottom—back-etched pyramid structure.

Figure 7(c) compares μPL spectra of single pyramids of the same sample before (top) and after 'back-etching'. The comparison shows that the 'back-etching' leads to an enhancement of the QD luminescence efficiency by more than three orders of magnitude. The luminescence from the GaAs QWR is also enhanced and appears at a higher energy for the 'back-etched' sample. (This shift is due to the tapering of the QWR and will be explained below.)

3.2.2. Bandgap structure of GaAs QWRs and AlGaAs VQWs. In order to further investigate the influence of the pyramid geometry on the optical spectra, we compare in figure 8(a) different μPL spectra of an $Al_{0.55}Ga_{0.45}As$ buffer layer without a GaAs QW. The top four spectra correspond to the three corners and the centre emission of an inverted pyramid,

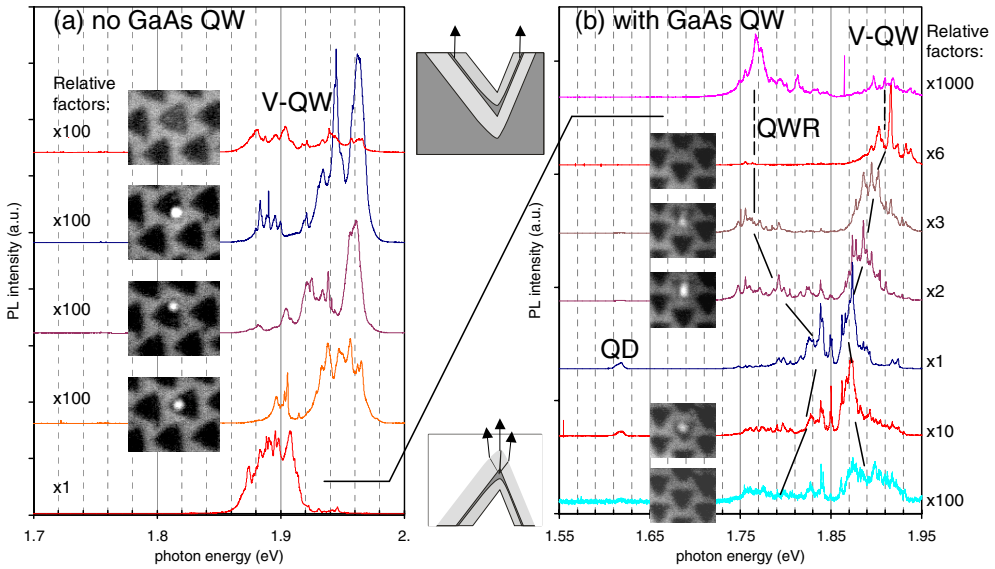

Figure 8. μPL spectra (10 K) and simultaneously recorded images of the PL emission comparing different spatial regions and pyramid geometries. (a) The sample without a GaAs QW shows only VQW emission. The top four spectra are taken from an inverted pyramid, the lowest one from a 'back-etched' pyramid. (b) Sample with GaAs QW showing contributions of QD, QWR and VQW. Top: inverted pyramid spectrum; lower six: spectra of a back-etched pyramid taken at different spatial positions arranged along a line crossing the centre of the pyramid (line-scan).

respectively, while the bottom spectrum shows the centre emission of a 'back-etched' pyramid. While the three spectra taken at an inverted pyramid corner are dominated by a high-energy contribution of the VQW luminescence, the spectrum taken at the centre position of the inverted pyramid (top spectrum) shows equally strong low- and high-energy VQW contributions and a reduced total PL intensity. The 'back-etched' sample (bottom) on the other hand shows a $\sim$100$\times$ enhanced PL intensity almost exclusively in the low-energy region of the VQW emission. These experimental results suggest that the VQW has a low-bandgap region near the pyramid centre and an increasing band gap towards the pyramid corners. Moreover, the low-energy emission from the pyramid centre is enhanced by a factor $>$100 when the measurement geometry is changed from an inverted pyramid to a 'back-etched' pyramid. This finding supports the importance of the 'lens effect' illustrated in figure 7(d), which strongly enhances luminescence contributions from the pyramid centre in the 'back-etched' geometry. This is in contrast to the standard inverted geometry, where the corner contributions dominate.

In a similar way, we can explain the difference between inverted and 'back-etched' pyramids containing a GaAs QW layer in figure 8(b). Here, the spectrum taken at the centre of an inverted pyramid (top) shows PL contributions of the QWR and the VQW at the same energies as the spectrum taken at the extreme corner of a 'back-etched' pyramid. This again indicates the predominance of the corner contribution in the inverted pyramid geometry. Following the μPL line-scan from the corner of the pyramid across the centre until the other side is reached (second spectrum from the top to bottom spectrum in figure 8(b)), we observe three different tendencies. First, as expected, the QD contribution is most intense in the spectrum taken at the exact centre of the pyramid. Second, similarly to the observations in figure 8(a), the VQW contribution shifts to lower energy as the centre of the pyramid is approached in

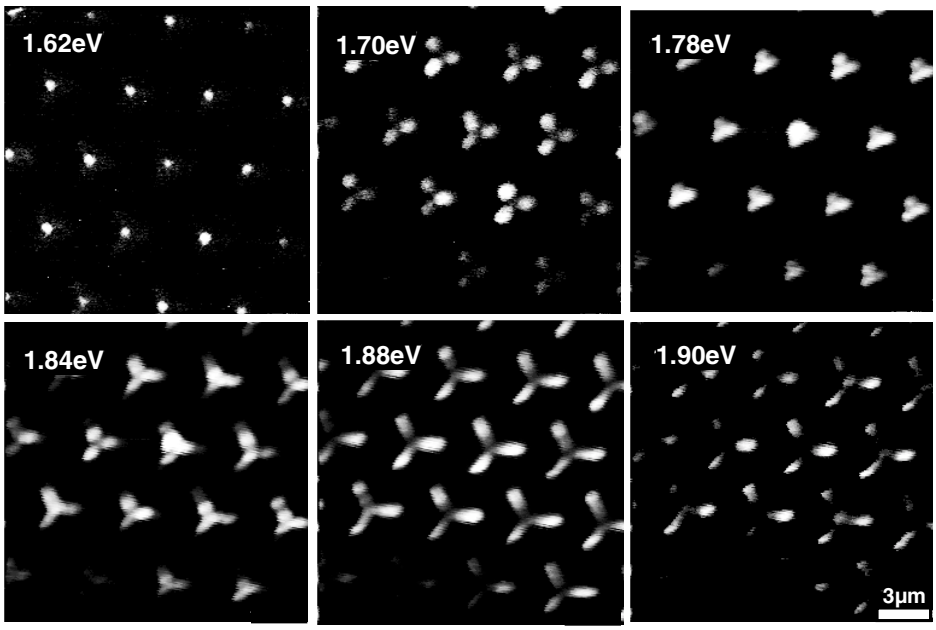

Figure 9. Series of plan view, monochromatic, low-temperature (10 K) CL images of the 'back-etched' pyramid sample of figure 8(b). The luminescence energy is given in the upper left corner of every image. (The image contrast has been enhanced for each image separately and is therefore not to scale between different images.)

either direction, indicating again the grading in the bandgap of the VQW. Finally, also the QWR peak is seen to shift, but in the opposite sense to the VQW peak as the pyramid centre is approached. This corresponds well to our structural results from x-AFM measurements (compare with figure 3), which show an increasing QWR thickness with increasing distance from the pyramid centre, corresponding to a band-gap decrease in that direction.

This inverse band-gap variation of GaAs QWRs and vertical Ga-rich AlGaAs QWs, which extend both along the three pyramid corners, is also easily observable in cathodoluminescence (CL) studies. Figure 9 shows a series of monochromatic CL images of the same 'back-etched' pyramid sample as in figure 8(b). At 1.62 eV, the first feature observable is emission from the pyramid centre, which corresponds to the QD. The QWR emission appears very weakly at 1.70 eV, located at the corners of the pyramid. As the emission energy increases up to 1.78 eV, it is seen to move toward the pyramid centre, demonstrating the band-gap tapering of the QWR. In the energy interval between 1.84 and 1.90 eV the opposite evolution can be observed. The emission starts at the centre of the pyramid and propagates towards the corners with increasing energy. This is direct evidence for the inverse band-gap tapering of the vertical AlGaAs QW as compared with that of the QWR.

A qualitative explanation for this inverse behaviour of the GaAs QWR and AlGaAs VQW is proposed. During the OMCVD, no growth takes place on the planar (111)B surfaces between the pyramidal patterns. Instead, all arriving growth species diffuse into and contribute to the growth inside the pyramids. The tapering of the GaAs QWR therefore reflects the direction of material transfer into the pyramids: species arrive from the border of the pyramid and diffuse towards its centre and are partially incorporated in the crystal on their way. This leads to a spatial growth rate gradient with a growth rate increasing in the direction from the pyramid

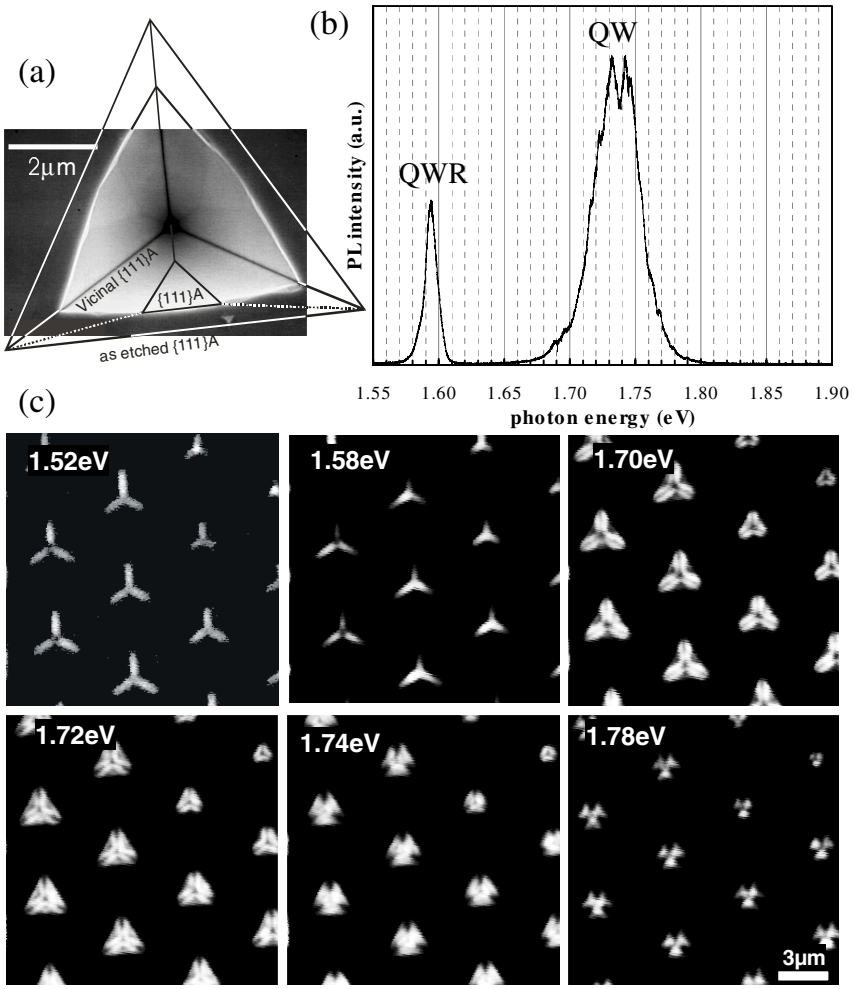

Figure 10. (a) SEM image and schematic reconstruction of the growth evolution on the pyramid sidewalls. (b) Single pyramid μPL spectrum and (c) series of plan view, monochromatic, low-temperature (10 K) CL images of a 'back-etched' pyramid sample with a thicker GaAs QW layer (15 s deposition time instead of 4 s) than the sample studied in figure 8(b). The imaging luminescence energy is given in the upper left corner of every image. (The image contrast has been enhanced for each image separately and is therefore not to scale between different images.)

centre to its border, which results in the observed QWR thickness tapering. However, for the AlGaAs VQW the implication is different: a higher growth rate implies a shorter diffusion time for the Ga adatoms to reach the corner, resulting in a VQW with a lower Ga concentration and a smaller width [33]. Therefore, the gradient in growth rate brings about a band-gap tapering in opposite directions for the GaAs QWR and the AlGaAs VQW.

3.2.3. Band-gap structure of the GaAs QW. Figure 10 shows how CL imaging can be used to understand the complex band-gap distribution of the GaAs QW in the pyramidal structures. The growth evolution of the pyramid sidewalls is schematically indicated in the SEM image of figure 10(a). During growth, each slower growing, as-etched (111)A sidewall is continuously

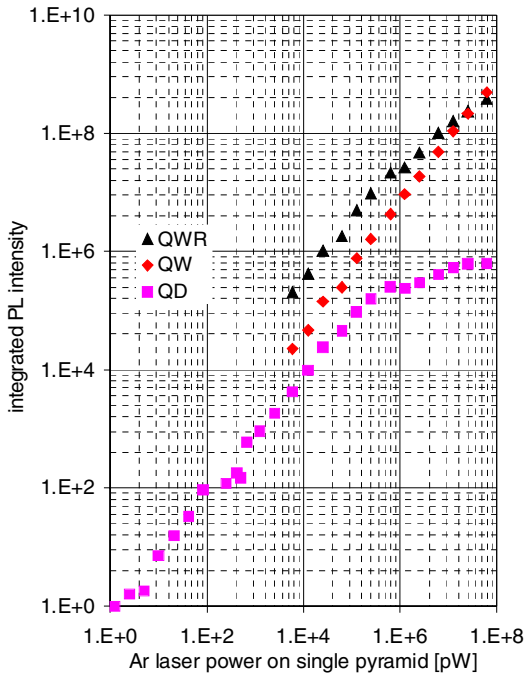

Figure 11. Integrated μPL peak intensities of the GaAs nanostructures as a function of excitation laser power.

replaced by a pair of faster growing vicinal (111)A planes. In the case of figure 10(a), a triangular portion of the original (111)A orientation is still visible in the centre of each sidewall. The luminescence that results from different sidewall facets is usually rather broad, as shown in figure 10(b). However, monochromatic CL imaging (figure 10(c)) can again be used to find the different spatial origins of each spectral component of the PL spectrum. The two first images (at 1.52 and 1.58 eV) show again the typical tapering of the GaAs QWRs: low-energy emission at the corners, which moves with increasing energy towards the pyramid centre. Between 1.70 and 1.78 eV, a complex evolution of the QW emission can be observed. At the lower energy regime, below 1.72 eV, the spatial intensity pattern observed corresponds well to the geometry of the vicinal (111)A faceted part of the sidewall in figure 10(a). Starting at 1.74 eV, a contrast inversion is observed, and the intensity pattern now suggests emission from the triangular (111)A planes at the centre of each sidewall. This observation is in agreement with the higher growth rate of the vicinal (111)A plane as compared to the as-etched (111)A, which results in a thicker QW layer and a lower QW band-gap energy for the former plane. Finally, between 1.74 and 1.78 eV a similar inward movement of the intensity pattern with increasing energy can be observed as for the QWRs, indicating a similar tapering for the GaAs QW layers.

3.3. Luminescence of single pyramidal quantum dots

3.3.1. Identification of QD luminescence. As mentioned above, we performed several experiments supporting our identification of the QD transition in the μPL spectra: the strong enhancement of QD luminescence in the 'back-etched' geometry (figure 7), the μPL line-scan of a 'back-etched' pyramid (figure 8) and the CL images (figure 9), which allow a direct

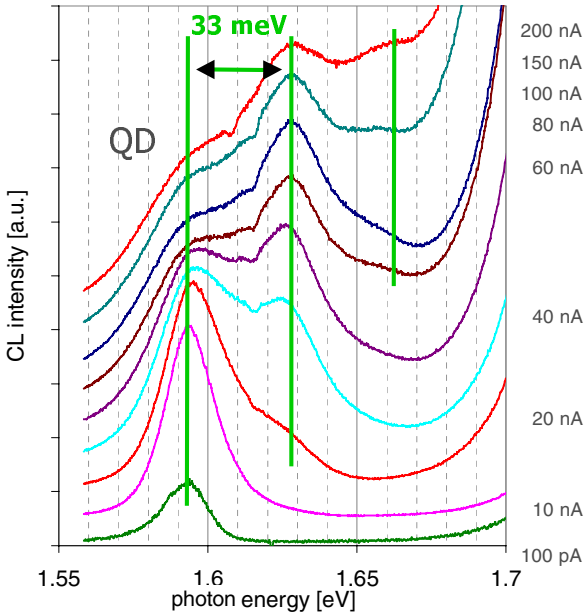

Figure 12. Evolution of low-temperature (10 K) CL spectra with increasing excitation current.

identification of the spatial origin within the pyramid of the QD luminescence.

To unambiguously confirm our peak assignment, we also probed consecutive pyramids along a cleaved edge. Due to the slight misalignment of the pyramid rows with respect to the cleavage direction, every pyramid is cleaved at a slightly different position. At a pyramid for which the centre is cleaved away, the PL emission of the QD should disappear, since the QD is situated at the centre of the pyramid. On the other hand, the other transitions should remain visible in the spectra of the pyramids whose centre is cleaved away. Exactly this behaviour is observed in the measurements, supporting the assignment of the QD PL line.

Furthermore, we performed excitation power dependent μPL measurements down to extremely low excitation powers. An example of a plot of integrated PL intensities versus excitation power is shown in figure 11. The QD luminescence intensity is seen to increase linearly with the excitation power over six orders of magnitude whereas it saturates strongly for higher power. The QWR luminescence intensity saturates less and at higher power, whereas the QW line intensity increases linearly with power over the whole tested range. Finally, in excitation power dependent CL (figure 12) and μPL measurements (not shown), excited QD levels have been observed, indicative of the zero-dimensional density of states of the QD.

3.3.2. Homogeneity of QD emission. A series of PL spectra evidencing the uniformity of single QD PL emission is displayed in figure 13. For different single QDs, separated by mm distances across the sample, the emission peak position varies only by about 4 meV. In large-area PL measurements, which integrate the emission of several 100 to several 1000 QDs, we observe PL line-widths of 10–15 meV.

For different epitaxies, we observe single QD PL line-widths ranging from 5 meV down to our resolution limit of 140 μeV. Recently, we were able to relate this variable line broadening and the complex spectral evolution of single QD PL spectra as functions of excitation power density to interactions of the QD-exciton with the shallow impurities in the QD environment.

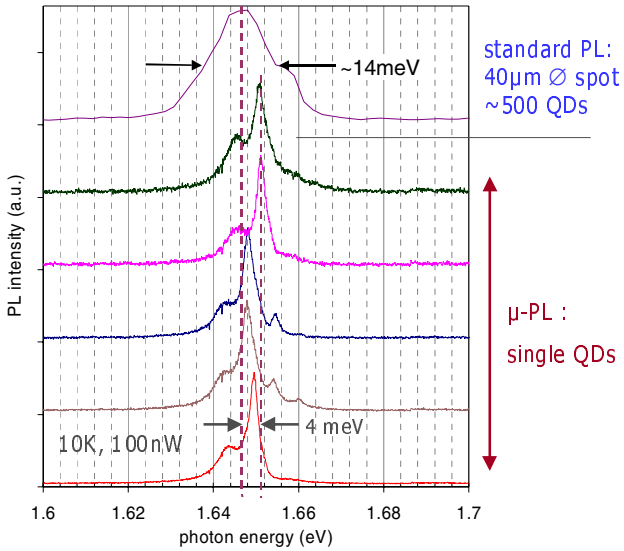

Figure 13. Comparison of single QD μPL spectra and a standard PL spectrum, integrated over ~500 individual QDs taken from back-etched pyramids.

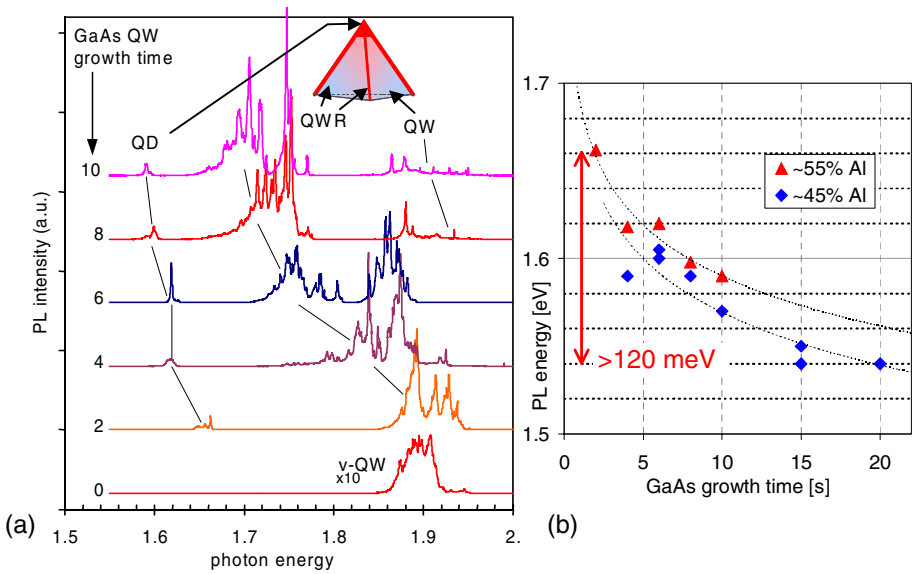

Figure 14. (a) μPL spectra of a series of samples with different GaAs QW deposition times. (b) Energy position of the QD emission as function of GaAs QW deposition time for two different Al mol fractions in the AlGaAs barrier layer.

A detailed description of these experiments and their theoretical explanation will be the subject of a separate publication.

3.3.3. Tailoring of QD band-gap energy. The effect of the thickness of the deposited GaAs QW layer on the μPL spectra of a single pyramid is shown in figure 14(a). In the spectrum

of a sample without GaAs QW (bottom), only the AlGaAs VQW luminescence is visible. Already for a 2 s deposition time of the GaAs QW, a QD luminescence feature is clearly visible at 1.66 eV. For this sample, the QD potential depth (distance to the next higher energy luminescence feature) is 200 meV. As the GaAs growth time is increased the GaAs QD and QWR features shift, as expected, to lower energy, while the AlGaAs VQW peak stays around 1.85–1.9 eV. Figure 14(b) gives an overview of the different QD band-gap energies which have been realized so far by changing the GaAs growth time or the AlGaAs barrier Al mol fraction. The QD band-gap energy could be tuned so far over an interval of 120 meV. However, an extension of this tuning range toward higher energies using shorter growth times and toward lower energies using the ternary InGaAs as QD material should be possible.

4. Conclusions and future directions

In conclusion, we have demonstrated that OMCVD growth in pyramidal recess patterns leads to the formation of very uniform QDs at the tip of each pyramid. The size and position of these QDs can be easily controlled. Due to the self-limited behaviour of the growth, this method is useful for fabricating large arrays of identical QDs. Such QD arrays would be useful, e.g., for studying dot-to-dot coupling effects.

A set of connected nanostructures inside the pyramids could be identified using cross-sectional atomic force microscopy. Our method of 'back-etching" allowed us to understand in detail the bandgap structure of this complex dot environment using optical spectroscopy techniques. Furthermore, an enhancement of the QD PL efficiency of more than three orders of magnitude could be observed due to more favourable reflection and refraction conditions in the inverted pyramid geometry.

In the future, special attention should be paid to several issues related to these QD heterostructures: the understanding of the interaction mechanisms of zero-dimensional carriers with other carriers inside or outside the dot as a function of the QD carrier density, and the determination of the carrier capture and recombination dynamics are a challenge due to the complex barrier structure of the dot. Realization of QD-based devices, e.g. light emitting diodes, should be facilitated in the back-etched geometry, due to the easy contacting of both sides of the junction that it offers. Finally, substrates prepared with optical holography techniques or electron beam lithography instead of conventional optical lithography should open the route to QD arrays with densities comparable to Stranski–Krastanow dots. Such high dot densities would be useful for optoelectronic applications, particularly QD lasers.

Acknowledgments

The authors gratefully acknowledge Amy Sadeghi for help with the sample preparation, Laurent Loubies and Frank Reinhardt for help with atomic force microscopy imaging and Fabrice Vouilloz and Daniel Oberli for help with optical measurements.

This project is supported by the Fonds National Suisse pour la Recherche Scientifique within PNR36 *Nanosciences*.

References

[1] Weisbuch C and Vinter B 1991 *Quantum Semiconductor Structures* (Boston: Academic)
[2] Arakawa Y and Sakaki H 1982 *Appl. Phys. Lett.* **40** 939–41
[3] Weisbuch C and Nagle J 1990 *Science and Engineering of One and Zero Dimensional Semiconductors. Proceedings of a NATO Advanced Research Workshop* (New York: Plenum) pp 309–16

[4] Lent C S, Tougaw P D, Porod W and Bernstein G H 1993 *Nanotechnology* **4** 49–57
[5] Fafard S 1997 *Photon. Spectra* **31** 160–4
[6] Orlov A O, Amlani I, Bernstein G H, Lent C S and Snider G L 1997 *Science* **277** 928–30
[7] Drexler H, Leonard D, Hansen W, Kotthaus J P and Petroff P M 1994 *Phys. Rev. Lett.* **73** 2252–5
[8] Oshinowo J, Nishioka M, Ishida S and Arakawa Y 1994 *Appl. Phys. Lett.* **65** 1421–3
[9] Marzin J Y, Gerard J M, Izrael A, Barrier D and Bastard G 1994 *Phys. Rev. Lett.* **73** 716–19
[10] Fafard S, Leonard D, Merz J L and Petroff P M 1994 *Appl. Phys. Lett.* **65** 1388–90
[11] Hessman D, Castrillo P, Pistol M E, Pryor C and Samuelson L 1996 *Appl. Phys. Lett.* **69** 749–51
[12] Grundmann M, Christen J, Ledentsov N N, Bohrer J, Bimberg D, Ruvimov S S, Werner P, Richter U, Gosele U, Heydenreich J, Ustinov V M, Egorov A, Zhukov A E, Kop'ev P S and Alferov I Zh 1995 *Phys. Rev. Lett.* **74** 4043–6
[13] Xie Q, Madhukar A, Ping C and Kobayashi N P 1995 *Phys. Rev. Lett.* **75** 2542–5
[14] Seifert W, Carlsson N, Miller M, Pistol M E, Samuelson L and Wallenberg L R 1996 *Prog. Cryst. Growth Characterization Mater.* **33** 423–71
[15] Solomon G S, Wu W, Tucker J R and Harris J S Jr 1998 *Physica* E **2** 1–4
[16] Brunner K, Bockelmann U, Abstreiter G, Walther M, Bohm G, Trankle G and Weimann G 1992 *Phys. Rev. Lett.* **69** 3216–19
[17] Bockelmann U, Roussignol P, Filoramo A, Heller W, Abstreiter G, Brunner K, Bohm G and Weimann G 1996 *Phys. Rev. Lett.* **76** 3622–5
[18] Wegscheider W, Schedelbeck G, Abstreiter G, Rother M and Bichler M 1997 *Phys. Rev. Lett.* **79** 1917–20
[19] Schedelbeck G, Wegscheider W, Bichler M and Abstreiter G 1997 *Science* **278** 1792–5
[20] Kapon E, Tamargo M C and Hwang D M 1987 *Appl. Phys. Lett.* **50** 347–9
[21] Bhat R, Kapon E, Hwang D M, Koza M A and Yun C P 1988 *J. Cryst. Growth* **93** 1–4
[22] Kapon E, Hwang D M and Bhat R 1989 *Phys. Rev. Lett.* **63** 430–3
[23] Colas E, Simhony S, Kapon E, Bhat R, Hwang D M and Lin P S D 1990 *Appl. Phys. Lett.* **57** 914–16
[24] Kapon E, Kash K, Clausen E M Jr, Hwang D M and Colas E 1992 *Appl. Phys. Lett.* **60** 477–9
[25] Tsukamoto S, Nagamune Y, Nishioka M and Arakawa Y 1993 *Appl. Phys. Lett.* **63** 355–7
[26] Wang X L, Ogura M and Matsuhata H 1995 *Appl. Phys. Lett.* **67** 3629–31
[27] Vouilloz F, Oberli D Y, Dupertuis M A, Gustafsson A, Reinhardt F and Kapon E 1997 *Phys. Rev. Lett.* **78** 1580–3
[28] Sugiyama Y, Sakuma Y, Muto S and Yokoyama N 1995 *Japan. J. Appl. Phys.* **34** 4384–6
[29] Hartmann A, Loubies L, Reinhardt F and Kapon E 1997 *Appl. Phys. Lett.* **71** 1314–16
[30] Reinhardt F, Dwir B and Kapon E 1996 *Appl. Phys. Lett.* **68** 3168–70
[31] Hartmann A, Ducommun Y, Loubies L, Leifer K and Kapon E 1998 *Appl. Phys. Lett.* **73** 2322–4
[32] Martinet E, Gustafsson A, Biasiol G, Reinhardt F, Kapon E and Leifer K 1997 *Phys. Rev.* B **56** R7096–9
[33] Biasiol G and Kapon E 1998 *Phys. Rev. Lett.* **81** 2962–5